Published OnlineFirst October 11, 2021; DOI: 10.1158/2326-6066.CIR-21-0031

Conditional PD-1/PD-L1 Probody Therapeutics Induce Comparable Antitumor Immunity but Reduced Systemic Toxicity Compared with Traditional Anti–PD-1/PD-L1 Agents

Hikmat H. Assi, Chihunt Wong, Kimberly A. Tipton, Li Mei, Ken Wong, Jennifer Razo, Chanty Chan, Bruce Howng, Jason Sagert, Michael Krimm, Linnea Diep, Andrew Jang, Margaret T. Nguyen, Nicole Lapuyade, Victoria Singson, Ruth Villanueva, Madan Paidhungat, Shouchun Liu, Vangipuram Rangan, Olga Vasiljeva, James W. West, Jennifer H. Richardson, Bryan Irving, Dylan Daniel, Marcia Belvin, and W. Michael Kavanaugh

ABSTRACT

Immune-checkpoint blockade has revolutionized cancer treatment. However, most patients do not respond to single-agent therapy. Combining checkpoint inhibitors with other immune-stimulating agents increases both efficacy and toxicity due to systemic T-cell activation. Protease-activatable antibody prodrugs, known as Probody therapeutics (Pb-Tx), localize antibody activity by attenuating capacity to bind antigen until protease activation in the tumor microenvironment. Herein, we show that systemic administration of anti–programmed cell death ligand 1 (anti–PD-L1) and anti–programmed cell death protein 1 (anti–PD-1) Pb-Tx to tumor-bearing mice elicited antitumor activity similar to that of traditional PD-1/PD-L1–targeted antibodies. Pb-Tx exhibited reduced systemic activity and an improved nonclinical safety profile, with markedly reduced target occupancy on peripheral T cells and reduced incidence of early-onset autoimmune diabetes in nonobese diabetic mice. Our results confirm that localized PD-1/PD-L1 inhibition by Pb-Tx can elicit robust antitumor immunity and minimize systemic immune-mediated toxicity. These data provide further preclinical rationale to support the ongoing development of the anti–PD-L1 Pb-Tx CX-072, which is currently in clinical trials.

Introduction

Immune checkpoints encompass multiple inhibitory and stimulatory mechanisms that are essential for maintaining self-tolerance and fine-tuning the duration and amplitude of immune responses. In patients with cancer, recombinant monoclonal antibodies (mAb) targeting inhibitory checkpoint molecules such as cytotoxic T-lymphocyte-associated antigen 4 (CTLA-4) or programmed cell death protein 1 (PD-1) and its ligand (PD-L1) can be effective strategies for reversing immune escape and elicit durable responses in a variety of indications (1, 2). A significant drawback to the administration of the mAb checkpoint inhibitors is the induction of systemic immune-related adverse events, which can be severe and life-threatening (3, 4). In addition to general inflammatory symptoms, patients treated with PD-1/PD-L1–targeting biologics can potentially develop life-threatening, organ-specific autoimmune reactions involving the gastrointestinal, hepatic, respiratory, endocrine, or central nervous systems (5–7). Although PD-1 expression is restricted to activated immune cells, its ligand PD-L1 can be found at low levels on a broad range of hematopoietic and nonhematopoietic cells such as those of the vascular endothelium, lung, liver, and muscle, indicating a potential role in maintaining the quiescence of T cells specific for self-antigens (8, 9). For some patients, the immune-related adverse events arising because of checkpoint inhibitor mAb therapy can necessitate dose reductions, delays, and discontinuations (10), which can be a significant impediment to successful treatment. In patients receiving multiple mAb checkpoint inhibitors, toxicities that limit therapy are not only more frequent but also more likely to be life-threatening and may require permanent discontinuation of checkpoint inhibitors (11). These clinical observations highlight the need for a new class of checkpoint inhibitors with reduced systemic toxicities.

In an attempt to decrease the toxicities of systemic mAb checkpoint inhibitor therapy, prior studies have examined the effectiveness of localized checkpoint inhibition (12, 13). These studies demonstrate that the localized delivery of checkpoint inhibitors can produce a therapeutic effect but do not establish whether this approach can also prevent systemic toxicity. It is reported that the therapeutic effect of checkpoint inhibition may require systemic activation of the immune system (14); therefore, it is not clear if the therapeutic and toxic effects can be separated with a local delivery strategy. We sought to test the hypothesis that localized PD-1/PD-L1 pathway inhibition can lead to effective antitumor immunity with minimal systemic enhancement of T-cell–mediated activity, including autoimmunity. To accomplish this, we generated constructs of Probody therapeutics (Pb-Tx) targeting the PD-1/PD-L1 pathway. Pb-Tx are a new class of proteolytically activated antibody prodrugs designed to minimize peripheral binding and promote tumor-specific activity (15, 16). The prodomain, an integral feature of Probody therapeutic technology, consists of a masking peptide that inhibits antigen binding connected to the antibody by a protease-cleavable linker (17). In healthy tissue where

CytomX Therapeutics, Inc., South San Francisco, California.

Note: Supplementary data for this article are available at Cancer Immunology Research Online (http://cancerimmunolres.aacrjournals.org/).

Corresponding Author: W. Michael Kavanaugh, CytomX Therapeutics, Inc., 151 Oyster Point Boulevard, Suite 400, South San Francisco, CA 94080. Phone: 650-763-9949; E-mail: mkavanaugh@cytomx.com

Cancer Immunol Res 2021;XX:XX–XX

doi: 10.1158/2326-6066.CIR-21-0031

Published OnlineFirst October 11, 2021; DOI: 10.1158/2326-6066.CIR-21-0031

protease activity is tightly regulated, the prodomain remains predominantly intact, preventing target binding (18). However, there is considerable evidence for upregulation of specific proteases in the tumor microenvironment compared with normal noncancerous tissue (19–22). For example, LeBeau and colleagues document active matriptase, a serine protease that can also activate the Pb-Tx presented in our study, in human colon cancer samples by using an active-site mAb, whereas normal colon samples show no evidence of this protease activity (19). Therefore, in the tumor microenvironment, which has elevated protease activity, the prodomain is designed to be cleaved and the masking peptide removed so that the Pb-Tx can engage the target, eliciting its intended therapeutic effect (17, 23).

We conducted a series of studies to investigate whether tumor-localized checkpoint inhibition with Pb-Tx can induce tumor growth inhibition and minimize peripheral immune-mediated toxicities. We show that PD-1/PD-L1–targeting Pb-Tx elicited therapeutic responses that were similar to results elicited with parental unmasked antibody and have demonstrated attenuated systemic target engagement and toxicity. These findings may allow for the development of checkpoint inhibitors with a wider therapeutic window and improved clinical utility.

Materials and Methods

Cell lines, antibodies, and recombinant proteins

Expi293F cells were purchased in 2013 from Life Technologies (catalog #A14527), subcultured, and cryopreserved per the vendor's recommendations and used for expression of recombinant proteins between passages 5 and 30. Human SAS cells were purchased in 2013 from the Japanese Collection of Research Bioresources (catalog #JCRB0260). MC38 cells were obtained in 2013 from Dr. Walter Storkus at the University of Pittsburgh, Pittsburgh, Pennsylvania. All cell lines were tested for a variety of viral and bacterial infectious agents, including *Mycoplasma*, by PCR prior to use (Idexx Laboratories IMPACT III PCR test). Human SAS cells and MC38 cells were maintained at fewer than 10 passages from the passage obtained from the vendor or source. Genotypic analysis for reauthentication purposes was not performed on the cell lines. Cells were cultured in RPMI-1640 (Thermo Fisher, catalog #72400047) or DMEM (Thermo Fisher, catalog #10564011) supplemented with 10% (v/v) fetal bovine serum (FBS; Thermo Fisher, catalog #10062147) as recommended by the vendors and maintained in a humidified atmosphere of 5% CO_2 at 37°C.

Mouse IgG2a clone C1.18.4 (catalog #BE0085, RRID:AB_1107771) was purchased from Bio X Cell. Human IgG4 isotype control was purchased from BioLegend (catalog #403701). All antibodies and Probody molecules targeted to PD-1 and PD-L1 were expressed at CytomX in Expi293F cells with the ExpiFectamine 293 Transfection Kit (Thermo Fisher catalog #A14524) per manufacturer's recommendation, purified to >95% purity and >95% monomer by protein A affinity chromatography (MabSelect SuRe, Cytiva, catalog #17543803) and size exclusion chromatography (Sepax SRT-10-SEC300) on an AKTA Pure system (Cytiva) using vendor's recommended protocols. All recombinant proteins were formulated in phosphate-buffered saline (PBS), pH 7.0 or 7.2, sterile filtered (0.2 micron), and confirmed to have an endotoxin level of <2 endotoxin unit (EU)/mg.

Antibody discovery

A PD-L1–blocking antibody was identified from a fully human single-chain variable fragment (scFv) phage-display library under contract by Creative Biolabs, using recombinant His-tagged human or mouse PD-L1 extracellular domain (Sino Biological, catalogs #10084-H02H and #50010-M08H, respectively). Five unique scFv clones that bound human PD-L1 (hPD-L1) extracellular domain were isolated and retested for specificity. Of these five, one cross-reactive clone was selected for affinity maturation and *in silico* assessment of immunogenicity. The light and heavy variable domains from the affinity-matured scFv were PCR-amplified and cloned into expression vectors based on pCDNA3 (Invitrogen) containing light (mouse and human kappa) and heavy (mouse IgG2a and human IgG1) constant regions, respectively. The affinity-matured lead clone (C5H9v2) was transiently expressed and purified as described above and confirmed to bind hPD-L1-Fc (R&D Systems, catalog #156-B7) and mouse PD-L1-Fc (R&D Systems, catalog #1019-B7) proteins by direct-binding enzyme-linked immunosorbent assay (ELISA), described below, with comparable affinity. C5H9v2 mAb was tested for specificity using the direct-binding ELISA described below and did not bind to several other related Fc-tagged proteins (both human and mouse proteins) including CTLA-4 (Sino Biological, catalogs #11159-H02H6 and #50503-M02H), PD-1 (Sino Biological, catalogs #10377-H02H and #50124-M02H), B7–1 (Sino Biological, catalogs #10698-H02H and #50446-M02H), CD137 (Sino Biological, catalogs #10041-H02H and #50811-M02H), OX40 (Sino Biological, catalogs #10481-H02H and #50808-M02H), and GITR (R&D Systems, catalogs #689-GR-100 and #524-GR-050; Supplementary Fig. S1). Amino acid sequences of murine C5H9v2 (muC5H9v2) mouse IgG2a (mIgG2a) are shown below.

muC5H9v2 mIgG2a heavy-chain amino acid sequence

EVQLLESGGGLVQPGGSLRLSCAASGFTFSSYAMSWVRQAP-
GKGLEWVSSIWRNGIVTVYADSVKGRFTISRDNSKNTLYLQM-
NSLRAEDTAVYYCAKWSAAFDYWGQGTLVTVSSAKTTAPSVY-
PLAPVCGDTTGSSVTLGCLVKGYFPEPVTLTWNSGSLSSGVHT-
FPAVLQSDLYTLSSSVTVTSSTWPSQSITCNVAHPASSTKVDKK-
IEPRGPTIKPCPPCKCPAPNLLGGPSVFIFPPKIKDVLMISLSPIVT-
CVVVDVSEDDPDVQISWFVNNVEVHTAQTQTHREDYNSTLR-
VVSALPIQHQDWMSGKEFKCKVNNKDLPAPIERTISKPKGSVR-
APQVYVLPPPEEEMTKKQVTLTCMVTDFMPEDIYVEWTNNG-
KTELNYKNTEPVLDSDGSYFMYSKLRVEKKNWVERNSYSCSV-
VHEGLHNHHTTKSFSRTPGK

muC5H9v2 mIgG2a light-chain amino acid sequence

DIQMTQSPSSLSASVGDRVTITCRASQSISSYLNWYQQKPGK-
APKLLIYAASSLQSGVPSRFSGSGSGTDFTLTISSLQPEDFATYYC-
QQDNGYPSTFGGGTKVEIKRADAAPTVSIFPPSSEQLTSGGASV-
VCFLNNFYPKDINVKWKIDGSERQNGVLNSWTDQDSKDSTYS-
MSSTLTLTKDEYERHNSYTCEATHKTSTSPIVKSFNRNEC

A humanized IgG4 anti-human PD-1 (anti–hPD-1; clone A1.5) was originally identified as a mouse hybridoma as described below. Six NZBWF1/J female mice (The Jackson Laboratory, catalog #100008) were immunized in the right flank with recombinant human PD-1 (Sino Biological, catalog #ABIN2181605) on days 0, 7, and 21. Serum was taken from immunized mice on day 28 and binding to HEK293-hPD-1 (cells transfected with an expression vector encoding human PD-1 (Origene, catalog # SC117011)) was measured. All six mice showed positive binding. Splenocytes were isolated from mice 1, 3, and 6 and fused with SP0 mouse B cells; likewise splenocytes were isolated from mice 2, 4, and 5 and fused with SP0 mouse B cells, giving rise to pools of hybridomas, m136 and m245. The hybridoma pools, m136 and m245, arising from the two fusions were plated for single clones, and clonal culture supernatants were assayed for antibodies capable of binding to HEK293-hPD-1, and not to untransfected HEK293, cells. Hybridoma clones expressing PD-1–specific antibodies were chosen

Published OnlineFirst October 11, 2021; DOI: 10.1158/2326-6066.CIR-21-0031

for further analysis. Clone A1.5 mAb was tested for specificity using the direct-binding ELISA described below and did not bind to several other related Fc-tagged proteins (both human and mouse proteins) including CTLA-4 (Sino Biological, catalogs #11159-H02H6 and #50503-M02H), PD-1 (Sino Biological, catalogs #10377-H02H and #50124-M02H), B7–1 (Sino Biological, catalogs #10698-H02H and #50446-M02H), CD137 (Sino Biological, catalogs #10041-H02H and #50811-M02H), OX40 (Sino Biological, catalogs #10481-H02H and #50808-M02H), and GITR (R&D Systems, catalogs #689-GR-100 and #524-GR-050; Supplementary Fig. S2).

A commercially available hamster antibody specific for mouse PD-1 (clone J43; Bio X Cell, catalog #BP0033-2) was converted into a mouse IgG2a isotype harboring the D265A mutation that minimized Fc effector activity. Briefly, DNA fragments encoding the variable light and the variable heavy domains of J43 were synthetically produced (GeneArt, Thermo Fisher) and cloned into an expression vector (based on pCDNA3, Invitrogen) containing the constant mouse kappa light and constant mouse mIgG2a domains, respectively.

Engineering of Probody molecules

A previous description for methods regarding the design and engineering of Probody therapeutic constructs has been published (17). Briefly, PD-1 and PD-L1 antibody and Fab fragments (made by digesting antibodies with Immobilized Papain, Thermo Fisher, catalog #20341, per the vendor's recommended protocol) were used to select masking peptides from bacterial surface–displayed peptide libraries. The bacterial library cells were subjected to repeated rounds of magnetically activated cell sorting with Protein A Dynabeads (Thermo Fisher, catalog #10008D) after incubation with unlabeled PD-1 or PD-L1 antibody and fluorescently activated cell sorting (FACSAria II, BD) after incubation with Alexa Fluor 488 labeled (Thermo Fisher, catalog #20000) PD-1 or PD-L1 antibody or Fab fragments to enrich for potential masking peptides. Protease-cleavable substrates were identified as previously described by screening cellular libraries of peptide substrates and optimized based on the aberrant expression of tumor-associated proteases (17). Several individual clones (96–192) from the final selected masking-peptide population were sequenced via Sanger sequencing (ELIM Biopharmaceuticals) and a set of 15 to 20 peptides, chosen based on their frequency in the sequenced set and sequence diversity, were assessed for masking activity. The chosen peptides alongside a cleavable linker were recombinantly fused to the N-terminus of the parental light chain to generate masked light chains by cloning synthetic DNA fragments between the signal peptide and the mature light chain in the light-chain plasmid. The proteins encoded by the antibody heavy chain and the set of masked light chains were expressed and purified as described above. The binding activity of the parental unmasked antibody and its masked derivatives was determined by the direct-binding ELISA described below. The presence of a functionally masking prodomain decreases the binding of activatable antibodies and manifests as an increase in the observed ELISA half-maximal effective concentration (EC_{50}) for the activatable antibody. The ratio of the observed EC_{50} of the activatable antibody to that of the original antibody is used as a measure of the masking activity of the prodomain and its component masking peptide. Amino acid sequences of CX-630 Pb-Tx are shown below.

CX-630 Pb-Tx heavy-chain amino acid sequence

EVQLLESGGGLVQPGGSLRLSCAASGFTFSSYAMSWVRQAP-GKGLEWVSSIWRNGIVTVYADSVKGRFTISRDNSKNTLYLQM-NSLRAEDTAVYYCAKWSAAFDYWGQGTLVTVSSAKTTAPSVY-PLAPVCGDTTGSSVTLGCLVKGYFPEPVTLTWNSGSLSSGVHT-FPAVLQSDLYTLSSSVTVTSSTWPSQSITCNVAHPASSTKVDKK-IEPRGPTIKPCPPCKCPAPNLLGGPSVFIFPPKIKDVLMISLSPIVT-CVVVDVSEDDPDVQISWFVNNVEVHTAQTQTHREDYNSTLR-VVSALPIQHQDWMSGKEFKCKVNNKDLPAPIERTISKPKGSVR-APQVYVLPPPEEEMTKKQVTLTCMVTDFMPEDIYVEWTNNG-KTELNYKNTEPVLDSDGSYFMYSKLRVEKKNWVERNSYSCSV-VHEGLHNHHTTKSFSRTPGK

CX-630 Pb-Tx light-chain amino acid sequence

QGQSGSIFCHMGVVVPQCANYGGGSSGGSGGSGGTSTSGR-SANPRGGGSDIQMTQSPSSLSASVGDRVTITCRASQSISSYLNW-YQQKPGKAPKLLIYAASSLQSGVPSRFSGSGSGTDFTLTISSLQP-EDFATYYCQQDNGYPSTFGGGTKVEIKRADAAPTVSIFPPSSEQ-LTSGGASVVCFLNNFYPKDINVKWKIDGSERQNGVLNSWTDQ-DSKDSTYSMSSTLTLTKDEYERHNSYTCEATHKTSTSPIVKSFN-RNEC

Protease activation of Pb-Tx molecules

Pb-Tx constructs were activated by cleavage with either urokinase-type plasminogen activator (uPA) or matriptase (MT-SP1) for *in vitro* binding and blocking assays. Test agents were incubated with 10% volume of uPA (R&D Systems, catalog 1310-SE) or MT-SP1 (catalog 3946-SEB) overnight (~16 hours) at 37°C. The concentration of protease used in both instances was >10 times that required to ensure complete cleavage of the substrate. Protease-digested samples were purified using MabSelect SuRe LX beads (GE Lifesciences, catalog #17-5474-01), buffer exchanged into PBS pH 7.2 by dialysis, and analyzed by sodium dodecyl sulfate polyacrylamide gel electrophoresis and high-performance liquid chromatography to verify that only cleaved Pb-Tx molecules are present.

Cytomegalovirus recall assay

Peripheral blood mononuclear cells (PBMC) from a cytomegalovirus (CMV)-positive donor (HemaCare) were plated at 2.5×10^5 cells per well in the presence of 4 μg/mL CMV antigen (Astarte Biologics, catalog #1004) and titrations of C5H9v2 (hPD-L1 mAb), CX-072 Pb-Tx, A1.5 mAb (hPD-1 mAb), CX-188 Pb-Tx or hIgG4 isotype control in a total volume of 200 μL DMEM (Thermo Fisher, catalog #10564011) supplemented with 10% (v/v) FBS (Thermo Fisher, catalog #10062147). Cells were incubated at 37°C in 5% CO_2. After 4 days, IFNγ levels were detected and quantified from the supernatant using an IFNγ ELISA kit (Life Technologies, catalog #KHC4021). The ELISA assay was performed according to the manufacturer's instructions. Absorbance was read at a wavelength of 450 nm using a microplate reader (BioTek ELx405). Data were graphed in Prism software version 6 (GraphPad Software). EC_{50} values were determined using nonlinear regression 4-PL analysis.

ELISAs

Direct-binding ELISA

Assessments of direct binding to recombinant PD-L1 derived from various species were performed using a sandwich ELISA in which immobilized recombinant proteins were incubated with titrations of the respective antibodies or Pb-Tx (± proteolytic preactivation with uPA or MT-SP1 protease). High-binding 96-well plates (Nunc MaxiSorp, Thermo Fisher) were coated overnight at 4°C with 50 μL of 1 μg/mL recombinant hPD-L1-Fc (R&D Systems, catalog #156-B7), cynomolgus monkey PD-L1-Fc (Sino Biological, catalog #90251-C02H), and rat PD-L1-Fc (Sino Biological, catalog #80450-R02H); mouse PD-L1-Fc (R&D Systems, catalog #1019-B7) was coated on plates at 0.5 μg/mL. Plates were washed six times with 300 μL in PBS,

Published OnlineFirst October 11, 2021; DOI: 10.1158/2326-6066.CIR-21-0031

0.05% Tween-20 (wash buffer), then blocked with PBS, 0.05% Tween, 1% bovine serum albumin (BSA blocking buffer) for 1 hour at room temperature. Plates were washed as before and incubated in 50 μL of an 11-point, three-fold serial dilution for antibodies targeting PD-L1 or PD-1 (C5H9v2 or J43v2, respectively) or Probody molecules (CX-072 or CX-284) accordingly. Activated Pb-Tx constructs were generated by incubating with uPA or MT-SP1 diluted in blocking buffer, for 1 hour at room temperature. Plates were washed as before, and 100 μL of anti-human IgG–horseradish peroxidase (HRP) conjugate, Fab-specific (Sigma-Aldrich, catalog #A0293-1ML; 1:3,000 dilution), or anti-mouse IgG–HRP conjugate (Sigma-Aldrich, catalog #A2554-1ML; 1:5,000 dilution) was added for 30 minutes at room temperature. Plates were washed as before and developed with 100 μL of chromogenic substrate 1-Step Ultra TMB-ELISA Substrate solution (Thermo Fisher, catalog #34029), and the reaction was stopped with 100 μL of 1N HCl. Absorbance was read at a wavelength of 450 nm using a microplate reader (BioTek). Data were graphed using Prism software. The EC_{50} values were determined using nonlinear regression and a 1-site–specific binding analysis.

Competition ELISA

The competition ELISA was performed as described above for the direct-binding ELISA with the following modifications. High-binding 96-well plates (Nunc MaxiSorp, Thermo Fisher) were coated with 50 μL of recombinant hPD-L1-Fc or recombinant mouse PD-1-Fc (R&D Systems, catalog #10-PD21). The associated human PD-1-Fc (Chimerigen Laboratories, catalog #CHI-HF-210PD1), human B7-1-Fc (Chimerigen Laboratories, catalog #CHI-HF-210CD80), or mouse PD-L1-Fc (R&D Systems, catalog #1019-B7) ligands were biotinylated using EZ-Link Sulfo-NHS-LC-Biotin (Thermo Fisher, catalog #21327) according to the manufacturer's instructions and dialyzed overnight with PBS buffer to remove unreacted Sulfo-NHS-LC-Biotin. Biotinylated PD-1-Fc (4 nmol/L) or PD-L1-Fc fusion (0.6 nmol/L) proteins were added to the wells and incubated for 1 hour at room temperature in the presence or absence of an 11-point, 3-fold serial dilution of respective blocking mAb, Pb-Tx, or protease-activated Pb-Tx. Plates were washed as described in the binding ELISA. Streptavidin–HRP conjugate (Thermo Scientific, catalog #21126) was added to the wells at a 1:5,000 dilution and incubated for 30 minutes at room temperature. Plates were washed as previously described and developed with 100 μL of chromogenic substrate 1-Step Ultra TMB-ELISA Substrate solution (Thermo Fisher, catalog #34029). The reaction was stopped with 100 μL of 1N HCl. Absorbance was read at a wavelength of 450 nm using a microplate reader (BioTek ELx405). Data were graphed in Prism software.

The ability of mouse PD-L1–specific antibody/Pb-Tx to block mouse PD-1/PD-L1 interactions was determined as described above with the exception that mouse PD-L1 was coated on plates at 0.5 μg/mL. Biotinylated mouse PD-1 was used at 2 nmol/L.

Cell-binding assay

Binding of hPD-L1 mAb (C5H9v2), CX-072 Pb-Tx, and preactivated CX-072 Pb-Tx to PD-L1–positive cells of human (SAS human cell line), mouse (MC38 mouse cell line), rat (Sprague Dawley rat peripheral blood $CD4^+$ T lymphocytes, BioIVT, catalog #RATWBLIHPO-M), and cynomolgus monkey (peripheral blood $CD4^+$ T lymphocytes, BioIVT, catalog #CYNWBLIHP-M) origin was evaluated by flow cytometry. Adherent cells were detached from flasks by rinsing once with PBS followed by Versene (Gibco, catalog #15040–066) at 37°C, washed with PBS, 2% FBS (staining buffer), and plated between 100,000 and 200,000 cells per well in a 96-well U-bottom plate and then pelleted at 200 × *g* for 3 minutes. Cells were incubated for 1 hour at 4°C with 50 μL of 8-point, 4-fold serial dilution of hPD-L1 mAb (C5H9v2), hPD-L1 Pb-Tx, or activated hPD-L1 Pb-Tx, serially diluted in staining buffer. After the incubation, the cells were washed three times with 200 μL of staining buffer and pelleted by centrifugation as described above. Anti-human IgG-AF647 (Jackson ImmunoResearch Laboratories, catalog #709-605-149) was added to cells at a 1:400 dilution for 30 minutes at 4°C. Cells were diluted with 200 μL of staining buffer and washed 3 times as previously outlined. Staining buffer (200 μL) was added to cells and cells analyzed on a flow cytometer (MACSQuant Analyzer 10, Miltenyi Biotec). Live cells were gated from forward/side scatter plots and the median fluorescence intensity (MFI) of AF647 was measured. Representative dot plots and gating are provided in Supplementary Fig. S3. Data were analyzed using FlowJo software (FlowJo, LLC) and graphed in Prism software (GraphPad Software). EC_{50} values were determined using three-parameter nonlinear regression analysis.

MC38 mouse tumor model

All *in vivo* work was performed in accordance with the Guide for the Care and Use of Laboratory Animals under a protocol approved by the Institutional Animal Care and Use Committee (protocols AP103; MC38 model and AP010; nonobese diabetic mouse model). CytomX Therapeutics, Inc. is an AAALAC accredited institution. Female C57BL/6 mice, obtained from Charles River Laboratories (RRID: IMSR_CRL:027), at 7 weeks of age were each inoculated with 1.5×10^6 MC38 cells subcutaneously into the right hind flank in a volume of 0.1 mL serum-free RPMI-1640 medium (Life Technologies). Tumor volumes and body weights were recorded twice weekly. Tumor dimensions were determined by caliper measurements, and tumor volume was calculated using the formula $(a \times b^2)/2$, where a is the longest and b is the shortest diameter. Tumor volumes were used to calculate percent tumor growth inhibition, expressed as $[1 - (T/C)] \times 100$, where T and C are the mean tumor volumes of the treated and control groups, respectively, on a given day. When mean tumor size reached 80 mm^3, mice were randomized into treatment groups. All test and control agents, including muC5H9v2, CX-603 Pb-Tx, CX-284 Pb-Tx, J43v2 mAb, and anti–CTLA-4 mAb (Bio X Cell, catalog #BP0164), were blinded and were administered by intraperitoneal injection beginning on day 1. The timing and dose differed in different experiments and can be found in figure legends for individual experiments. All mice were examined daily for health status and were euthanized by CO_2 inhalation when tumors reached 2,000 mm^3, body weight loss exceeded 20%, another humane endpoint was met, or at study termination.

Western capillary electrophoresis

Tumor, spleen, and liver were harvested 4 days after dose from mice withMC38 tumor dosed with 5 mg/kg of either CX-630 or the parental antibody and frozen. Frozen tissues (15–35 mg) were cut on the ThermalTray slim low-profile platform over dry ice (BioCision, catalog #BCS-252). Immediately after cutting, each sample was placed in a cryostat (−20°C). Immediately after taking each sample out from the cryostat, 100 μL of Pierce IP Lysis Buffer (Thermo Fisher, catalog #87788) with 1X Halt Protease Inhibitor Cocktail and 0.5 M ethylenediaminetetraacetic acid (EDTA; Thermo Fisher, catalog #78438) was added. Protein was then extracted using the Barocycler 2320EXT (Pressure BioScience) for 40 cycles of 30 seconds at 35,000 psi and 10 seconds at ambient pressure at 20°C. The samples were centrifuged at 18,500 × *g* for 15 minutes at 4°C, and the supernatant was collected. Samples were frozen at −80°C until use. Activated and

Published OnlineFirst October 11, 2021; DOI: 10.1158/2326-6066.CIR-21-0031

intact anti–PD-L1 Pb-Tx was detected using an anti-idiotype primary antibody (clone 17G1, CytomX Therapeutics) and anti-mouse secondary antibody (ProteinSimple, catalog #042-205). Capillary electrophoresis was performed on the Sally Sue instrument (ProteinSimple) following standard instrument protocol. Probody concentrations in tumor/tissue were obtained from Compass software peak area data in SoftMax Pro software where Basic Endpoint protocol was used to back-calculate against active and intact anti–PD-L1 Pb-Tx by 4-parameter logistic standard curves.

CD8 immunohistochemistry

C57BL/6 mice bearing MC38 tumors (average volume of 80 mm^3) were treated with muC5H9v2 mAb, CX-630 Pb-Tx, or isotype control (5 mg/kg) on days 0, 3, and 7. On day 8, tumors were excised, fixed in formalin, and embedded in paraffin blocks. CD8 immunohistochemical analysis was performed by Cureline, Inc. Briefly, 5 μm sections were cut, deparaffinized, and rehydrated followed by antigen retrieval using an EDTA buffer. Sections were washed and incubated in a blocking solution. Primary staining was performed with a 200-fold dilution of rabbit anti-CD8 antibody (Abcam, catalog #ab217344) or isotype control (Abcam, catalog #ab172730) in staining buffer (PBS with 0.5% Tx-100 and 1% FBS) for 1 hour at room temperature. After several washes, tissue sections were stained with an anti-rabbit HRP-conjugated secondary antibody for 20 minutes at room temperature (Dako, catalog #P0448). After a final wash step, the slides were incubated with a 3,3′-diaminobenzidine chromogen for 10 minutes at room temperature. After rinsing, slides were counterstained with hematoxylin, dehydrated, cleared, and mounted. Brightfield whole-tissue scans where performed on the slides using the Vectra Polaris Imaging System (Akoya Biosciences) at a 20× magnification. Snapshots images were captured digitally from the scan at 10× magnification using Phenochart software version 1.0.

Mouse plasma IgG2a capture ELISA

The plasma concentrations of muC5H9v2 mAb, CX630 Pb-Tx, or mouse IgG2a isotype control were measured by a capture ELISA using immobilized anti-mouse IgG2a(a), a haplotype-specific antibody to detect the test agents in a C57BL/6 background. Briefly, high-binding 96-well plates (Nunc MaxiSorp, Thermo Fisher) were coated overnight at 4°C with 60 μL of 4 μg/mL anti-mouse IgG2a(a) (clone 8.3, BD Biosciences). Plates were washed with wash buffer (PBS, 0.05% Tween-20), then blocked with a PBS/1% BSA solution for 1 hour at room temperature. Samples were diluted 1:20, 1:200, or 1:2,000 in blocking buffer. Plates were washed as before and incubated in 60 μL of the test agents: an 11-point, 2-fold serial dilution (concentration range, 0.488–500 ng/mL) performed in replicates of muC5H9v2 mAb or CX630 Pb-Tx diluted in blocking buffer, for 1 hour at room temperature. Plates were washed as before and 60 μL of anti-mouse IgG2a–biotin conjugate (clone 8.3, BD Biosciences, catalog #553502) in blocking buffer was added for 1.5 hours at room temperature. Plates were washed as before and 60 μL of streptavidin–HRP diluted 1:5,000 (Pierce, catalog #21140) in block buffer was added for 30 minutes at room temperature. Plates were washed as before and developed with 100 μL of chromogenic substrate 1-Step Ultra TMB-ELISA Substrate Solution (Thermo Fisher, catalog #34029). The reaction was stopped with 100 μL of 1N HCl. Absorbance was read at a wavelength of 450 nm using a microplate reader (BioTek ELx405). Data were graphed in Prism software, and concentrations were interpolated using 4-parameter logistic nonlinear regression analysis.

Target occupancy assay

Female C57BL/6 mice with established subcutaneous MC38 tumors 60 to 120 mm^3 in size were given a single intraperitoneal injection of muC5H9v2 mAb, CX-630 Pb-Tx, or mouse IgG2a control antibody at 5, 3, 1, or 0.3 mg/kg. Four days after dosing, terminal bleeds were taken with a minimum of 200 μL (+ EDTA) for flow cytometry analysis and 100 μL (lithium heparin) for processing to plasma and stored at −80°C for exposure assessment in single aliquots. Blood was taken from the remaining untreated control tumor-bearing mouse to serve as a negative control and for compensation control for flow cytometry analysis. The amount of muC5H9v2 or CX-072 bound to the surface of $CD4^+$ T cells was assessed by flow cytometry. A 50 μL sample of whole blood from each animal was incubated with 5 μL of mouse FcR block (Miltenyi Biotec; catalog #130-092-575) in duplicate wells for 10 minutes at 4°C. The following dilutions were prepared in 1:10 mouse FcR block in Stain Buffer BSA (BD Biosciences, catalog #554657) and incubated for 1 hour: For the *ex vivo* samples, 55 μL of PBS was added to one set of wells. For the saturated samples, 55 μL of 40 μg/mL mouse PD-L1 antibody (C5H9v2) was added to one set of duplicate wells. For background control, 55 μL of 40 μg/mL of mouse IgG2a isotype control was added to the wells of untreated animals. Red blood cells were lysed using 1,100 μL of RBC Lysis Solution (Miltenyi Biotec; catalog #130-094-183) for 10 minutes. Cells were pelleted at 300 × *g* for 5 minutes. Cells were washed once with RBC lysis buffer followed by two washes with 200 μL of stain buffer. Anti-mouse H+L IgG-biotin (Jackson ImmunoResearch Laboratories, catalog #715-065-151, RRID:AB_2340785) at 1:500 dilution was added to the wells for 30 minutes. Cells were washed twice with 200 μL of stain buffer and incubated with a cocktail of anti-mouse CD4-Pacific Blue and anti-mouse CD45-APC-Cy7, and 1:500 dilution of streptavidin-phycoerythrin (streptavidin-PE; Invitrogen catalog #12-4317-87) for 30 minutes. Cells were washed twice with 200 μL of stain buffer before 7-aminoactinomycin D (7-AAD, BD Bioscience catalog #559925) was added to the wells to detect dead cells. Cells were analyzed on a flow cytometer (MACSQuant, Miltenyi Biotec). Live lymphocytes were gated from forward/side scatter plots, negative 7-AAD, and positive CD45 gates. The MFI of PE was measured in the $CD4^+$ cells and graphed in Prism software. Background MFI was subtracted from all samples. Percent target occupancy was determined using the following equation: (*ex vivo* MFI of PE)/(saturated MFI of PE) × 100.

Nonobese diabetic diabetes model

Female nonobese diabetic (NOD)/ShiLtJ mice (The Jackson Laboratory, stock #001976) were maintained with free access to standard food and water. Nine-week-old female mice confirmed to be prediabetic (negative for glucosuria) were randomized and dosed with muC5H9v2 mAb, CX-630 Pb-Tx, or mouse IgG2a (BIW) by intraperitoneal injection. In the combination study, 5-week-old prediabetic female NOD mice were injected intraperitoneally with muC5H9v2 mAb, CX-630 Pb-Tx, or mIgG2a at 10 mg/kg on days 0, 4, and 7 in combination with either anti–CTLA-4 clone 9D9 (Bio X Cell, catalog #BP0164) or mIgG2b (Bio X Cell, catalog #BP0086) at 10 mg/kg. Body weights and urinary glucose levels were monitored daily. Urinary glucose was monitored daily using a glucose test strip (Diastix; Bayer Corporation). Blood obtained by means of a tail nick was tested for glucose with an Alpha TRAK 2 test strip inserted into a glucometer (Abbott Animal Care, now owned by Zoetis). Any animal with detectable glucose in urine (≥100 mg/dL) was immediately tested for blood glucose level. Animals with blood glucose levels ≥250 mg/dL for 2

Published OnlineFirst October 11, 2021; DOI: 10.1158/2326-6066.CIR-21-0031

consecutive days were designated as diabetic and euthanized by CO_2 inhalation.

Statistical analysis

Statistical analysis was performed using GraphPad Prism software version 6 (GraphPad Software). All the data points represent the mean ± SD. Differences in tumor size between groups were assessed by one-way analysis of variance using the Dunnett correction for multiple comparisons. A P value of <0.05 was considered statistically significant. Kaplan–Meier survival plots were generated with Prism and were analyzed using the survival analysis tool, which performs a log-rank test.

Results

Characterization of PD-L1–neutralizing antibody

A phage-displayed scFv library was used to identify clones that bound specifically to PD-L1. Positive clones were characterized for their affinity and binding specificity. From this pool, a clone was selected for further development (C5H9v2; Supplementary Table S1). The variable light and heavy domains of the lead antibody were cloned into expression vectors for hIgG4 (S228P; C5H9v2) and mIgG2a muC5H9v2. The equilibrium binding affinity of C5H9v2 hIgG4 mAb to recombinant human, monkey, rat, and mouse PD-L1 fusion protein was determined by ELISA; nanomolar affinity was observed (**Fig. 1A**; ref. 24). Similar subnanomolar EC_{50} values were obtained for on-cell binding to PD-L1–expressing human, monkey, rat, and mouse cells by flow cytometry (Supplementary Table S2). The capacity of this antibody to inhibit the interaction of PD-L1 with its two known receptors, PD-1 and B7-1 (25, 26), was also evaluated by ELISA. The addition of single-digit nanomolar concentrations of C5H9v2 mAb abrogated all binding of PD-1 [half-maximal inhibitory concentration (IC_{50}) = 0.65 nmol/L] or B7-1-Fc fusions (IC_{50} = 0.46 nmol/L) to plate-bound PD-L1 (**Fig. 1B** and **C**).

Next, the ability of C5H9v2 mAb to enhance T-cell activation was evaluated by an antigenic recall assay. This assay measures IFNγ

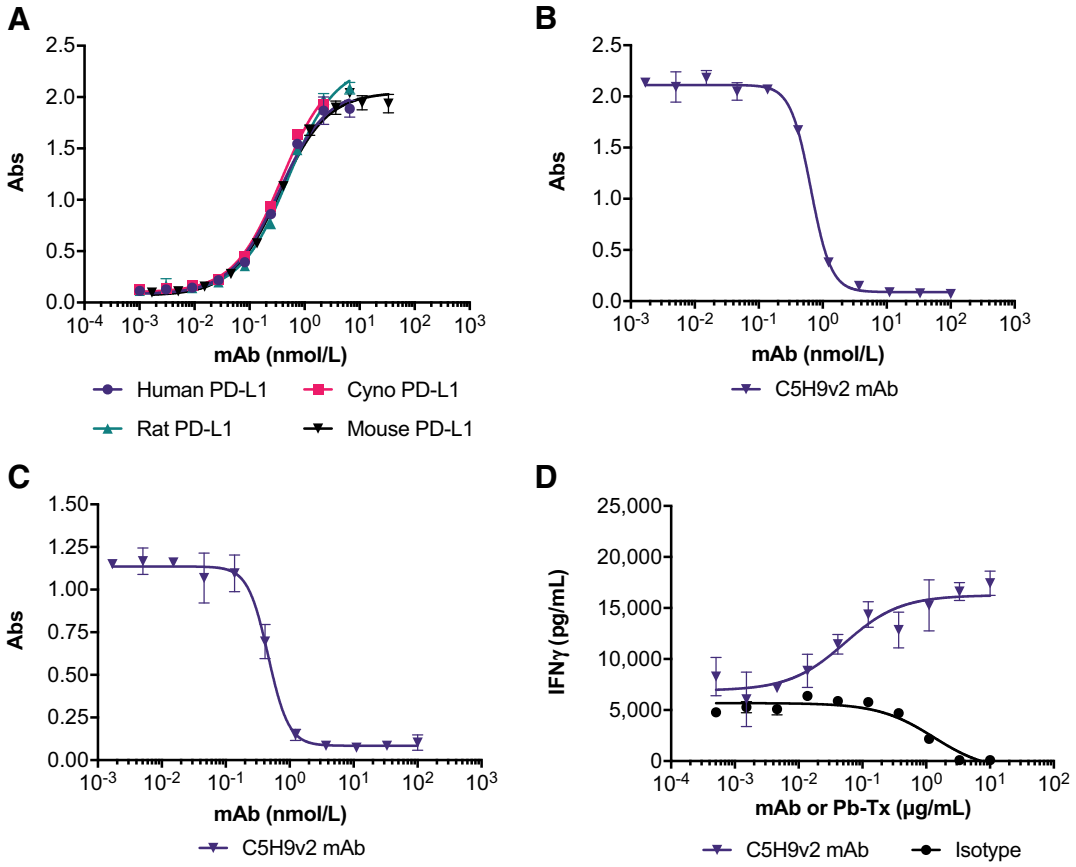

Figure 1.

C5H9v2 mAb is a high-affinity blocker of PD-L1 and can potentiate T-cell responses. **A,** The capacity of C5H9v2 hIgG4 mAb to bind and block immobilized PD-L1 was evaluated in an ELISA format. Serial dilutions of C5H9v2 mAb were incubated with recombinant plate-bound PD-L1-Fc fusion protein of human, mouse, rat, or cynomolgus monkey origin. Bound antibody was detected using an anti-human HRP-conjugated secondary antibody and is shown in relation to the concentration. Data shown are representative of 3 independent experiments. Serial dilutions of C5H9v2 mAb were added to wells containing biotinylated hPD-1 (**B**) or hB7-1 (CD80; **C**) protein and plate-bound PD-L1-Fc to measure blocking capacity. The binding of hPD-1 or hB7-1 to PD-L1 was detected using a streptavidin–HRP conjugate. Data shown are representative of 3 independent experiments. **D,** Blockade of PD-L1 by C5H9v2 mAb enhanced IFNγ production in a CMV recall assay. CMV-positive hPBMCs were plated at 350,000 cells/well in media containing serial dilutions of C5H9v2 mAb or isotype control and stimulated with 4 μg/mL CMV lysate for 4 days, at which point IFNγ was measured in the supernatants by ELISA. Data shown are representative response from one donor (n = 3 donors tested) of 3 independent experiments. All data points represent the mean ± SD. Abs, absorbance; Cyno, cynomolgus monkey; hB7-1, human B7-1; hPBMC, human peripheral blood mononuclear cell.

Published OnlineFirst October 11, 2021; DOI: 10.1158/2326-6066.CIR-21-0031

secretion by CMV-specific T cells derived from human PBMCs in response to CMV peptide–pulsed antigen-presenting cells. Blockade of the PD-1/PD-L1 interaction enhances IFNγ secretion by CMV-specific memory T cells when reexposed to CMV antigens (27). Human PBMCs from CMV-positive donors were stimulated with lysate from CMV-infected cells for 4 days in the presence of increasing concentrations of antibody. An increase of IFNγ production was observed when C5H9v2 mAb was present (EC_{50} = 0.35 nmol/L) compared with an isotype-matched control antibody, consistent with an enhanced antigen-specific T-cell response (**Fig. 1D**). Collectively, this data set validates C5H9v2 as a high-affinity neutralizing antibody to PD-L1 suitable for further development as a Pb-Tx.

Engineering of PD-1/PD-L1–targeting Pb-Tx

C5H9v2 IgG and antigen-binding fragment (Fab) constructs were used to identify potential masking peptides from a diverse bacterial peptide-display library, as described previously (28). Peptides conferring the desired masking properties were paired with protease-cleavable linker substrates to create unique prodomains as illustrated in Supplementary Fig. S4. The degree of functional attenuation achieved by a given prodomain can be expressed as a ratio of the antigen-binding EC_{50} values of the Pb-Tx and the nonmasked parental antibody. A Pb-Tx composed of C5H9v2 with a prodomain conferring the desired degree of masking and protease cleavability was designated CX-072 and selected for further development. This Pb-Tx is currently being studied in a phase I/II clinical trial (NCT03013491).

To further characterize the blockade of PD-1/PD-L1 with Pb-Tx in mouse models, we simultaneously generated muC5H9v2, a surrogate chimeric antibody composed of a mouse IgG2a constant region and the variable domains of the C5H9v2 mAb. Given the differences in observed affinity of C5H9v2 mAb to mouse PD-L1 and hPD-L1, masks for muC5H9v2 were generated such that the binding affinity of the surrogate Pb-Tx construct for mouse PD-L1 (**Fig. 2**) was comparable with that of CX-072 to hPD-L1 (Supplementary Table S1). In addition, the protease-sensitive substrate linker was optimized to match cleavability by mouse and human proteases. For the purposes of clarity, the Pb-Tx construct engineered for mouse studies was designated CX-630. All mAbs and Pb-Tx used in this report are described in **Table 1**.

In the absence of proteases, CX-630 Pb-Tx bound to mouse PD-L1 with approximately 120-fold lower affinity compared with muC5H9v2 mAb [equilibrium dissociation constant (K_D) of 47.23 vs. 0.40 nmol/L, respectively] and showed a corresponding reduced capacity to inhibit PD-1/PD-L1 interactions (IC_{50} of 94.9 nmol/L vs. 0.44 nmol/L, respectively; **Fig. 2A** and **B**). To evaluate whether affinity for antigen is restored after removal of the mask, CX-630 was activated overnight with the recombinant human protease uPA. *In vitro*, the binding and blocking properties of uPA-activated CX-630 were indistinguishable from those of the parental muC5H9v2 antibody (**Fig. 2A** and **B**). The physiologic significance for attenuated binding to PD-L1 was demonstrated in the CMV recall assay, where the Pb-Tx CX-072 was less potent in inducing IFNγ than the C5H9v2 hIgG4 mAb (**Fig. 2C**).

To further characterize localized blockade of the PD-1/PD-L1 pathway, Pb-Tx targeting PD-1 were developed using the anti-murine PD-1 J43 antibody (29). The binding affinity for the murine-specific antibody (J43v2) and that for its Pb-Tx derivative (CX-284) to mouse PD-1 were evaluated by ELISA. Although the J43v2 mAb bound with subnanomolar affinity (K_D = 0.627 nmol/L), CX-284 exhibited a 20-fold reduction in its ability to bind to mouse PD-1 relative to J43v2 (K_D = 11.54 nmol/L; **Fig. 3A**; ref. 30). Furthermore, the Pb-Tx molecule exhibited an attenuated capacity to block the interaction of PD-1 with PD-L1 (IC_{50} = 35.04 nmol/L) relative to the parental antibody J43v2 (IC_{50} = 2.17 nmol/L; **Fig. 3B**). *In vitro* activation of CX-284 by recombinant proteases restored full binding and blocking activity (IC_{50} = 2.77 nmol/L; **Fig. 3A** and **B**). To evaluate the impact of masking PD-1 on human cells, a CMV recall assay was performed using an antibody and Pb-Tx targeting the hPD-1 receptor (A1.5 mAb and CX-188 Pb-Tx). The ability of the Pb-Tx to enhance IFNγ production by CMV-positive human PBMCs was attenuated compared with the A1.5 antibody (EC_{50} = 1.67 nmol/L vs. 0.047 nmol/L; **Fig. 3C**).

Table 1. List of mAbs and Pb-Tx.

Molecule	Target	Isotype
C5H9v2 mAb	h/mPD-L1	hIgG4 S228P
CX-072 Pb-Tx	h/mPD-L1	hIgG4 S228P
muC5H9v2 mAb	h/mPD-L1	mIgG2a
CX-630 Pb-Tx	h/mPD-L1	mIgG2a
A1.5 mAb	hPD-1	hIgG4 S228P
CX-188 Pb-Tx	hPD-1	hIgG4 S228P
muJ43v2 mAb	mPD-1	mIgG2a D265A
CX-284 Pb-Tx	mPD-1	mIgG2a D265A

Abbreviations: hPD-1, human programmed cell death protein 1; hPD-L1, human programmed cell death ligand 1; mPD-1, mouse programmed cell death protein 1; mPD-L1, mouse programmed cell death ligand 1.

Targeted intratumoral blockade of the PD-1/PD-L1 pathway is an effective therapeutic strategy

Pb-Tx are engineered to be activated by proteases within the tumor microenvironment, allowing the activated Pb-Tx to bind locally while limiting peripheral engagement of the target antigen. Using this approach, we set out to determine whether localized intratumoral blockade of the PD-1/PD-L1 axis was sufficient for therapeutic activity. Single-agent efficacy studies were conducted in the MC38 mouse tumor model. Syngeneic C57BL/6 mice with established subcutaneous MC38 tumors were randomly assigned for treatment with muC5H9v2 mAb, CX-630 Pb-Tx, or mouse IgG2a isotype as a control. As illustrated in **Fig. 4A**, the PD-L1 Pb-Tx CX-630 elicited comparable therapeutic activity relative to the unmasked parental antibody, achieving maximal tumor growth inhibition of >60% ($P \leq 0.05$ for each vs. isotype, one-way analysis of variance).

To substantiate the results that we observed with PD-L1–targeting Pb-Tx, antitumor activity of a PD-1–targeting Pb-Tx was also characterized. Mice with established MC38 tumors were randomized and treated with PD-1–blocking J43v2 mAb, CX-284 Pb-Tx, or control mouse IgG1. Administration of CX-284 Pb-Tx resulted in activity in the MC38 model comparable to that of the parental J43v2 mAb, with percent tumor growth inhibition at day 24 of 81.8% and 82.7%, respectively (**Fig. 4B**; ref. 31). To investigate whether the anti–PD-1 Pb-Tx was also effective in combination therapy, MC38-bearing mice were treated with CX-284 Pb-Tx and an anti–CTLA-4 antibody. In this combination, CX-284 Pb-Tx elicited antitumor activity comparable to that of the unmasked parental antibody, J43v2 (**Fig. 4C**). Finally, treatment with CX-284 Pb-Tx monotherapy was sufficient for the induction of long-lasting protective immunity (immunologic memory) in mice that responded completely to an initial challenge. Rechallenging these mice with MC38 tumor cells resulted in prompt rejection, whereas experimentally naïve mice of the same age developed tumors (**Fig. 4D**). These results are similar to those reported for other PD-1/PD-L1 pathway inhibitors and are consistent with Pb-Tx

Published OnlineFirst October 11, 2021; DOI: 10.1158/2326-6066.CIR-21-0031

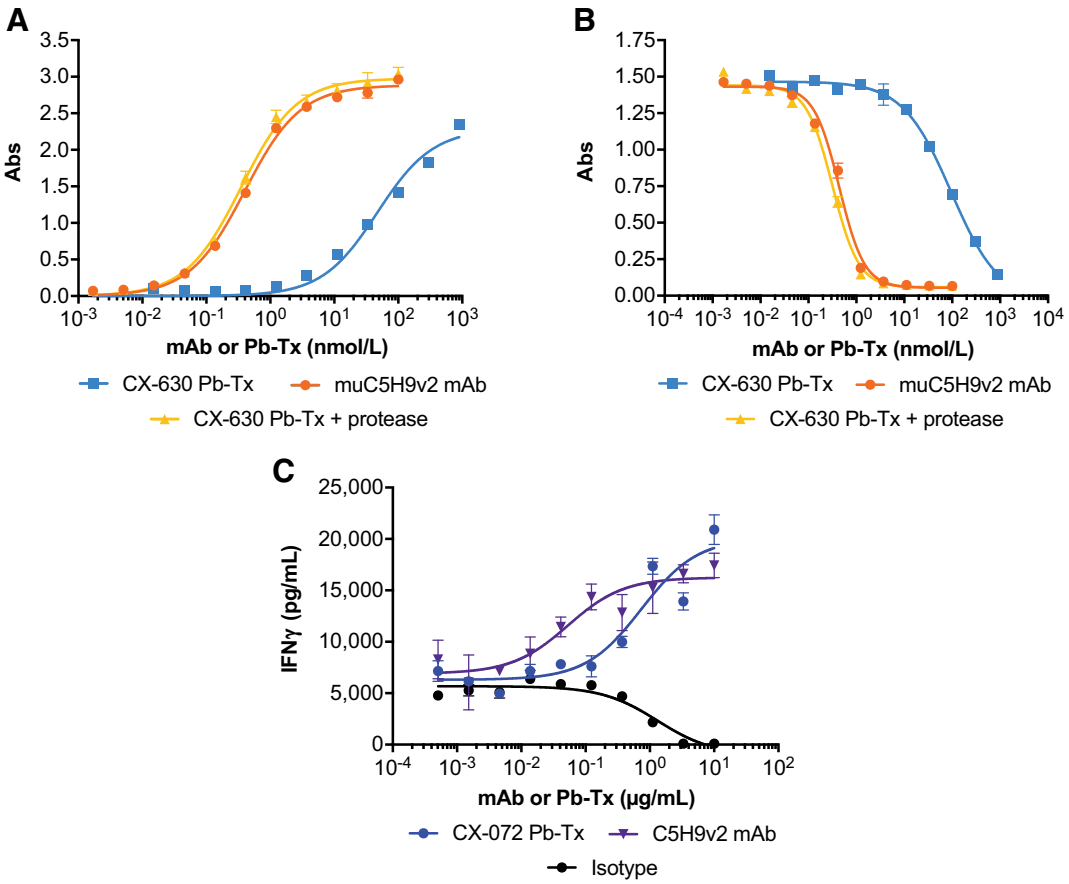

Figure 2.

PD-L1–targeting Pb-Tx exhibits protease-dependent blocking activity *in vitro*. **A,** Serial dilutions of muC5H9v2 mAb or Pb-Tx CX-630, either pretreated or not with recombinant human protease (uPA), were incubated with immobilized PD-L1-Fc. The binding affinity of the agents was measured using an anti-mouse HRP-conjugated secondary antibody and is shown in relation to the concentration. Data shown are representative of 3 independent experiments. **B,** The capacity of CX-630 to block ligand binding was impaired relative to the parental unmasked antibody, as indicated by a competition ELISA assay. Dilutions of muC5H9v2 mAb or CX-630, either pretreated or not with iPA, were mixed with biotinylated PD-1 in a well that was precoated with PD-L1-Fc. The amount of PD-1 bound to PD-L1 was measured using a streptavidin–HRP conjugate and is shown in relation to the amount of blocking antibody or Pb-Tx. Data shown are representative of 3 independent experiments. **C,** CMV-positive human PBMCs were plated at 250,000 cells/well and stimulated with 5 μg/mL CMV lysate in the presence of CX-072 Pb-Tx, C5H9v2 mAb, or isotype control for 4 days, at which point IFNγ was measured in the supernatants by ELISA. Data shown are representative response from one donor ($n = 3$ donors tested) of 3 independent experiments. All data points represent the mean ± SD. Abs, absorbance.

effectively targeting PD-L1 (32). Taken together, the results suggest that the localized inhibition of the PD-1/PD-L1 axis in the tumor microenvironment is an effective therapeutic strategy.

Intratumoral mechanism of action of Pb-Tx directed to PD-L1

We next performed a series of experiments to elucidate the mechanism of action of PD-1/PD-L1–directed Pb-Tx in the tumor microenvironment. We examined whether T-cell expansion could be detected in tumors from CX-630–treated animals. Immunohistochemical analysis revealed an increase in the infiltration of $CD8^+$ T cells into the tumor, indicating an active T-cell response that was comparable to that seen in mice treated with the parental PD-L1 antibody muC5H9v2 (**Fig. 4E**).

Next, we conducted *in vivo* studies to evaluate whether a PD-L1–targeting Pb-Tx can be unmasked in tumors while remaining intact in the normal tissue. A capillary electrophoresis immunoassay was used to measure the concentration of activated CX-630 in tumor, spleen, and liver tissues. After 4 days of circulation, we observed significant accumulation of the activated anti–PD-L1 Pb-Tx construct in the tumor homogenate relative to normal tissues (**Fig. 4F**). These results suggest that CX-630 can be activated intratumorally, but remain substantially intact in the periphery. In agreement with these findings, we have previously demonstrated that CX-072 radiolabeled with the positron emission tomography isotope zirconium-89 accumulates specifically in PD-L1–expressing tumors, whereas limited uptake, similar to the nonbinding Pb-Tx control, was detected in normal murine peripheral lymphoid tissues (33). Taken together, these results demonstrate that PD-L1–targeted Pb-Tx can be unmasked by tumor-associated proteases and produce the expected effect of increasing tumor-infiltrating $CD8^+$ T cells, but remain predominantly masked in the periphery.

Pb-Tx show reduced systemic inhibition of the PD-1/PD-L1 pathway

Pb-Tx are engineered to remain intact in healthy tissues, with minimal engagement to antigen that is expressed in the periphery.

Published OnlineFirst October 11, 2021; DOI: 10.1158/2326-6066.CIR-21-0031

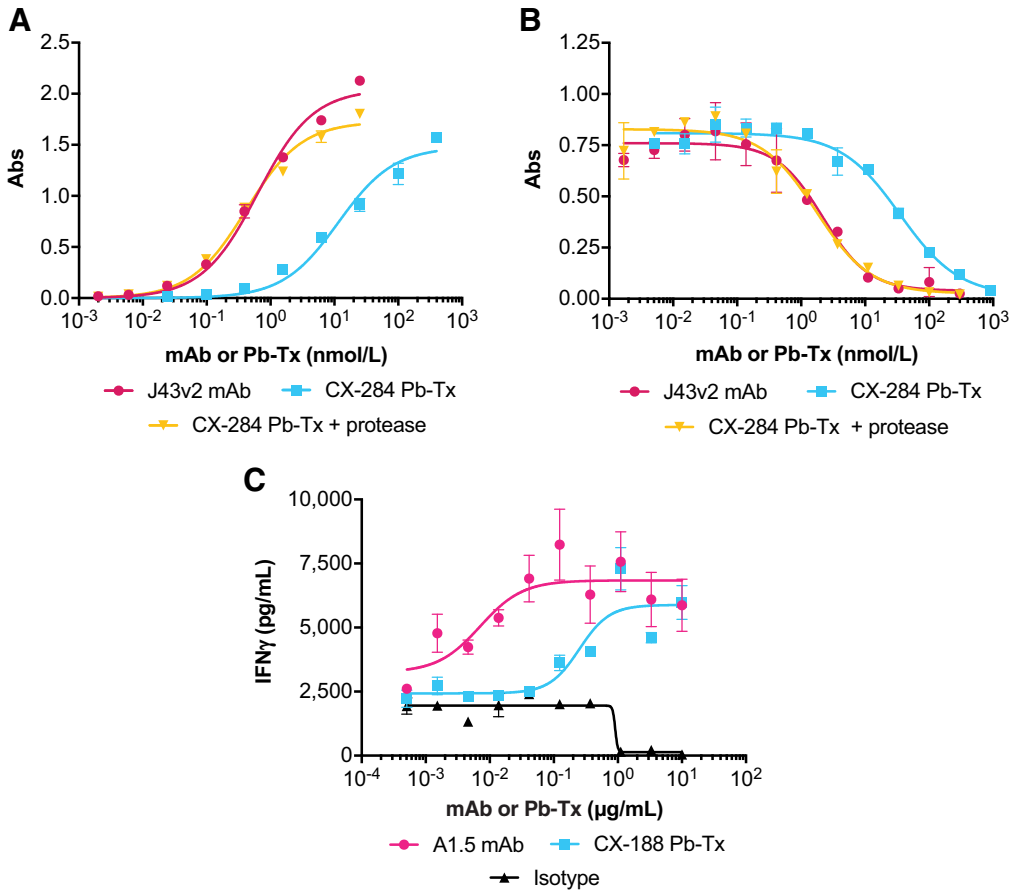

Figure 3.

Pb-Tx targeting the PD-1 pathway exhibits attenuated, protease-dependent binding. **A,** CX-284 Pb-Tx binds mouse PD-1 with a lower affinity relative to the parental antibody, as indicated by direct ELISA. Serial dilutions of J43v2 mAb or Pb-Tx CX-284, either pretreated or not with recombinant human protease (uPA), were incubated with immobilized mouse PD-1. The binding affinity of the agents was detected using an anti-mouse HRP-conjugated secondary antibody. Data shown are representative of 3 independent experiments. **B,** The ability of CX-284 to block ligand binding is impaired relative to the parental antibody, as indicated by a competition ELISA assay. Biotinylated PD-L1 was added to wells coated with PD-1-Fc in the presence of serially diluted J43v2 mAb or CX-284 (± uPA preactivation). The amount of bound PD-L1 was measured using a streptavidin–HRP conjugate and is shown in relation to the amount of blocking antibody or Pb-Tx. Data shown are representative of 3 independent experiments. **C,** CMV-positive human PBMCs were plated at 250,000 cells/well and stimulated with 4 μg/mL CMV lysate in the presence or absence of the human PD-1–targeted antibody A1.5, the human PD-1–targeted Pb-Tx CX-188, or isotype control. After 4 days, the level of IFNγ was measured in the supernatants by ELISA. Data shown are representative response from one donor ($n = 3$ donors tested) of 3 independent experiments. All data points represent the mean ± SD. Abs, absorbance.

Having established that these therapeutics effectively inhibit the PD-1/PD-L1 pathway locally in tumors, the potential for peripheral (non-tumor) engagement with PD-L1 by the Pb-Tx was evaluated in the MC38 tumor model. Binding of the muC5H9v2 mAb or CX-630 Pb-Tx to PD-L1 expressed on the surface of peripheral blood $CD4^+$ T cells was measured as a function of dose and concentration in tumor-bearing mice. Binding to PD-L1 on peripheral $CD4^+$ T cells was concentration-dependent. However, distinct exposure–response profiles were observed for the two molecules, with higher concentrations required for binding of CX-630 Pb-Tx to achieve a lower maximal binding capacity (**Fig. 5A**). The impaired binding of CX-630 Pb-Tx to peripheral T cells is consistent with the finding that the drug remains largely masked and in its prodrug form in the blood of tumor-bearing mice for 4 days after administration.

Given that NOD mice have a genetic predisposition to developing T-cell–mediated autoimmune diabetes at a young age, they serve as a useful model for studying autoimmunity. The onset of diabetes in this mouse strain can be accelerated by blocking the PD-1/PD-L1 interaction (34). In very young NOD mice, CTLA-4 blockade can also induce autoimmune diabetes (35). We used this model to test the hypothesis that the incidence of autoimmune disease associated with systemic PD-1/PD-L1 checkpoint inhibition can be attenuated when the inhibitory antibody is administered in a Pb-Tx format. Nine-week-old female NOD mice were given a single intraperitoneal injection of muC5H9v2 mAb, CX-630 Pb-Tx, or mouse IgG2a control at 0.3, 1, or 3 mg/kg, respectively. Blood glucose was measured in all mice testing positive for urinary glucose. Early-onset diabetes was observed in ≥50% of 9-week-old female NOD mice dosed with the anti–PD-L1 muC5H9v2 at 1 mg/kg; it was not observed in any of the mice treated at the same dose of the anti–PD-L1 Pb-Tx CX-630 and was observed in only 25% of mice treated with 3 mg/kg (**Fig. 5B**). Statistical significance was achieved in the 1 mg/kg cohorts as indicated by a log-rank test. These results demonstrate that the Pb-Tx induces a lower incidence of autoimmunity than the unmasked anti–PD-L1 antibody in the

Published OnlineFirst October 11, 2021; DOI: 10.1158/2326-6066.CIR-21-0031

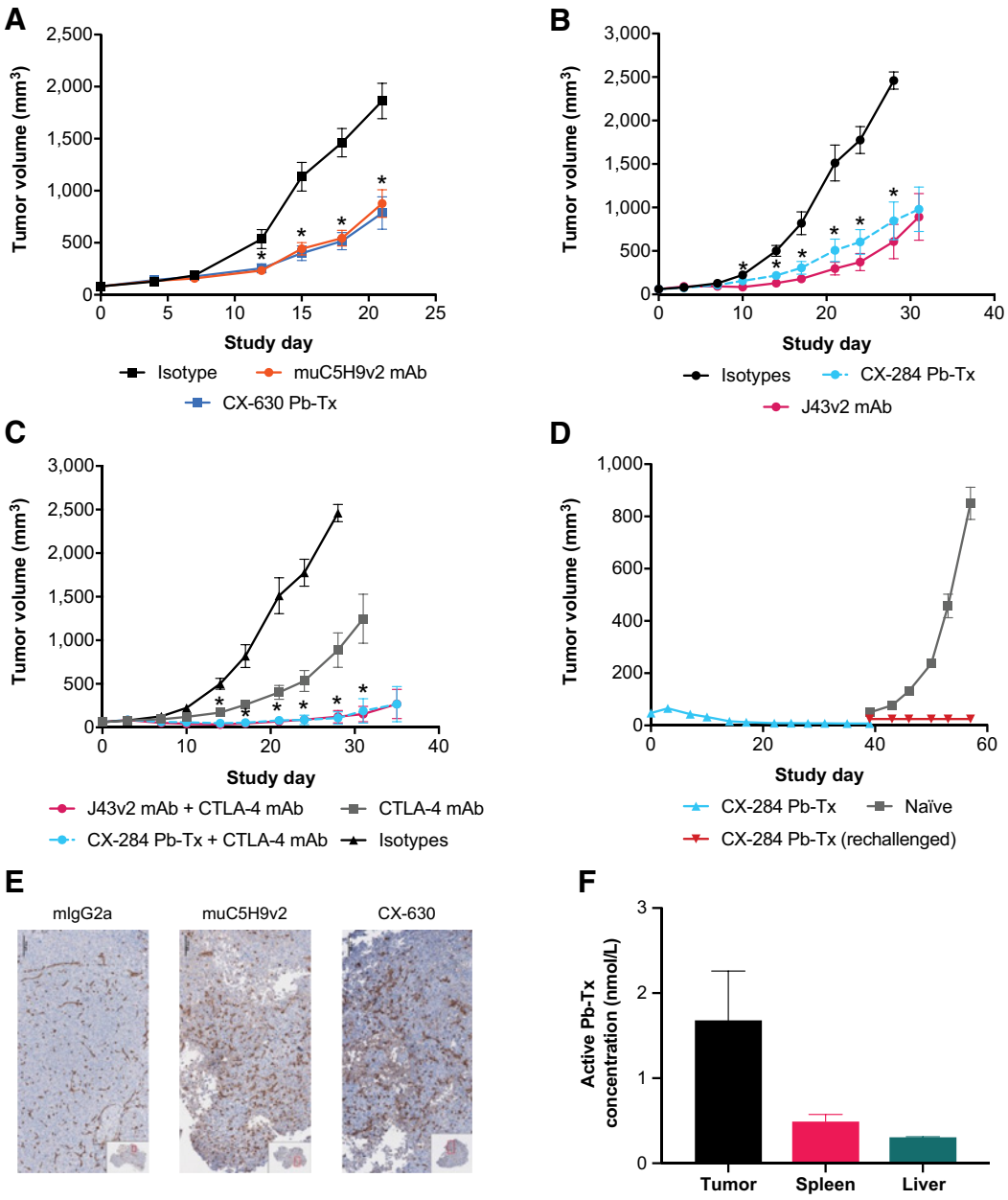

Figure 4.

Systemically administrated PD-1/PD-L1 Pb-Tx are preferentially activated in protease-rich tumor microenvironments eliciting antitumor immune responses that are comparable with responses of the unmasked antibodies. **A,** Growth of syngeneic MC38 tumors in C57BL/6 mice was monitored in response to the anti–PD-L1 muC5H9v2 or the PD-L1–targeted Pb-Tx CX-630. Mice bearing MC38 tumors of ∼80 mm^3 were treated by intraperitoneal injection starting day 0 with 5 mg/kg, twice weekly for 3 weeks; $n = 10$/group. Data shown are representative of 4 independent experiments. *, $P \leq 0.05$ for each versus isotype, one-way analysis of variance with Dunnett test. **B,** Female C57BL/6 mice with established MC38 tumors, average volume 45 to 80 mm^3, were randomized into groups of 10 mice and administered anti–PD-1 (J43v2), PD-1–targeted Pb-Tx (CX-284), or control mIgG2a by intraperitoneal injection twice weekly at 10 mg/kg for a total of 6 injections. Tumor volumes were monitored and are shown as a function of time. Data shown are representative of 4 independent experiments. *, $P \leq 0.05$ for each versus isotype, one-way analysis of variance with Dunnett test. **C,** Tumor-bearing mice were treated with a combination of anti–CTLA-4 (10 mg/kg, twice weekly for 3 weeks) and JV43v2 or CX-284 (10 mg/kg, twice weekly for 3 weeks) and monitored for tumor growth. Data shown are representative of 3 independent experiments. *, $P \leq 0.05$ for each versus CTLA-4 mAb group, one-way analysis of variance with Dunnett test. **D,** Mice bearing MC38 tumors (∼40 mm^3) in the right flank were treated with CX-284 (10 mg/kg, twice weekly for 3 weeks; $n = 35$). Of that cohort, mice that had undergone complete tumor regression because of CX-284 treatment were rechallenged with a subcutaneous injection of MC38 cells in the left flank and monitored for tumor growth without additional therapy alongside a naïve control group. Data shown are pooled from 3 independent experiments. **E,** C57BL/6 mice bearing MC38 tumors roughly ∼80 mm^3 in size were treated with 5 mg/kg of muC5H9v2, CX-630, or isotype control on days 0, 4, and 7. On day 8, the tumors were excised, fixed with formalin, and embedded in paraffin. Microphotographs of tumor-tissue sections stained with an anti-CD8 antibody are shown at 10× magnification. **F,** Tumor and normal tissues were harvested from MC38 tumor–bearing mice 4 days after treatment with a single dose of CX-630 (5 mg/kg). Concentrations of activated Pb-Tx were determined by Western capillary electrophoresis using an anti-idiotype antibody. Data shown are representative of 3 independent experiments.

Published OnlineFirst October 11, 2021; DOI: 10.1158/2326-6066.CIR-21-0031

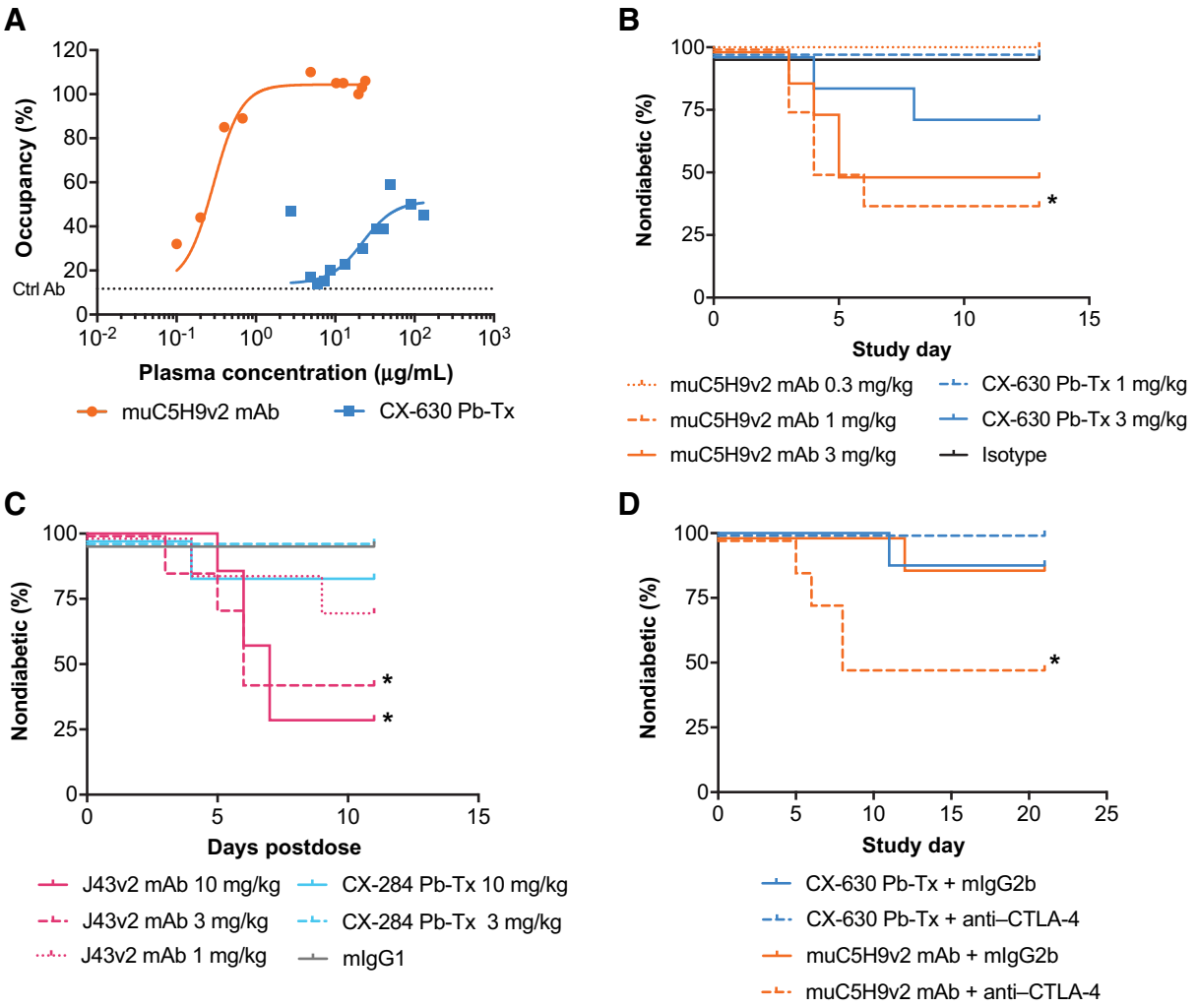

Figure 5.

Pb-Tx targeting the PD-1/PD-L1 pathway protects peripheral T cells from checkpoint blockade. **A,** PD-L1 receptor occupancy on circulating $CD4^+$ T cells is shown as a function of plasma concentration from MC38 tumor–bearing mice treated systemically with a single dose of muC5H9v2 mAb or CX-630 Pb-Tx. Dose levels were 0.3, 1, 3, or 5 mg/kg; $n = 3$ mice/group. Blood collected 4 days later was analyzed for $CD4^+$ T-cell surface–bound muC5H9v2 or CX-630 by flow cytometry. Plasma concentrations of each article were determined by ELISA and plotted against the surface occupancy data. The dotted line represents nonspecific staining based on mIgG2a isotype–treated group (control antibodies). Data shown are representative of 3 independent experiments. **B,** The incidence of diabetes was monitored in NOD mice following a single administration of muC5H9v2 or CX-630 at the indicated doses, or control mIgG2a at 1 mg/kg; $n = 8$ mice/group. Urinary glucose levels were monitored daily using a glucose test strip. Mice with glucose ≥5.55 mmol/L (100 mg/dL) were tested immediately for blood glucose and were deemed diabetic if exhibiting blood glucose levels ≥13.88 mmol/L (250 mg/dL) for 2 consecutive days. Data shown are representative of 2 independent experiments. *, $P \le 0.05$ for each dose versus Pb-Tx, log-rank test. **C,** Incidence of diabetes in NOD mice following a single administration of J43v2, CX-284, or mIgG1 isotype at various doses; $n = 7$ mice/group. Data shown are representative of 4 independent experiments. *, $P \le 0.05$ for each dose versus Pb-Tx, log-rank test. **D,** Incidence of diabetes in NOD mice following a single dose of muC5H9v2 mAb or CX-630 Pb-Tx (10 mg/kg) combined with anti–CTLA-4 or its respective isotype control (10 mg/kg). *, $P \le 0.05$ for each dose versus Pb-Tx, log-rank test. Ctrl Ab, control antibody group; mIgG, mouse immunoglobulin G.

NOD mouse model and are consistent with the finding of reduced peripheral engagement of PD-L1 on circulating T cells depicted in **Fig. 5A**.

The potential for autoimmune disease induction by a PD-1–targeting antibody and Pb-Tx was also evaluated. As was observed for the anti–PD-L1 mAb, the onset of diabetes in NOD mice was accelerated by administration of the anti–PD-1 mAb J43v2. Early-onset diabetes was observed in 71%, 57%, and 29% of NOD mice dosed with the anti–PD-1 at 10, 3, and 1 mg/kg, respectively, whereas no diabetes was seen in mice that were administered mouse IgG1 at 10 mg/kg or the anti–PD-1 Pb-Tx CX-284 at 3 mg/kg. Mice dosed with 10 mg/kg CX-284 had a 14% incidence of early-onset diabetes (**Fig. 5C**).

To evaluate the onset of autoimmunity in a combinatorial treatment setting, studies were performed in younger mice, which are reportedly less sensitive to PD-1/PD-L1 inhibition but more sensitive to CTLA-4 blockade (35, 36). Administration of muC5H9v2 mAb in combination with anti–CTLA-4 to 5-week-old NOD mice resulted in a 50% incidence of early-onset diabetes (**Fig. 5D**), whereas no diabetes was observed in mice dosed with a combination of CX-630 Pb-Tx and anti–CTLA-4. Taken together, these studies demonstrate that PD-1 and PD-L1–directed Pb-Tx induce a lower incidence of systemic

Published OnlineFirst October 11, 2021; DOI: 10.1158/2326-6066.CIR-21-0031

autoimmunity both as single agents and in combination therapy than do unmasked antibodies.

Discussion

Prior studies using viral vectors to restrict the delivery of checkpoint inhibitors suggest that localizing PD-1 pathway blockade to the tumor microenvironment can produce a therapeutic effect, but these studies did not establish whether this approach effectively localizes checkpoint blockade or reduces the toxicity. For example, intratumoral administration of myxoma virus engineered to express the soluble form of PD-1 induces antitumor $CD8^+$ T-cell responses that are more effective compared with administration of the combination of unmodified myxoma virus and systemic PD-1–targeted antibodies. The only reported measurement of autoimmune toxicity in this model was vitiligo, which is significantly reduced in mice treated with myxoma virus expressing soluble PD-1 (12). In a similar approach, intratumoral delivery of an attenuated oncolytic measles virus expressing anti–PD-1 or anti–CTLA-4 mAb results in similar efficacy compared with systemic administration, although no assessments of systemic exposure or toxicity were made (37). Using an oncolytic vaccinia virus as a shuttle for checkpoint inhibitors, Kleinpeter and colleagues (38) demonstrate that intratumoral accumulation of a PD-1 antibody is improved compared with subcutaneous or intratumoral delivery of recombinant antibodies, and this is associated with growth inhibition of MCA205 immune-competent tumors (38). Using a human epidermal growth factor receptor 2 (HER2)–targeting adeno-associated virus to redirect the biodistribution of anti–PD-1, Reul and colleagues (39) demonstrate preferential expression of an encoded anti–PD-1 scFv-Fc in tumor tissue relative to the serum or liver. The antitumor activity of this approach is modest in BALB/c mice bearing subcutaneous RENCA-HER2/neu tumors, and no characterizations of systemic activity were made (39). Although these reports provide evidence for potential therapeutic benefit with localized PD-1/PD-L1 checkpoint inhibition, the effects on systemic activity were not established. In addition, viral vectors have significant drawbacks over systemic administration of recombinant antibodies, in that the levels and duration of expression are largely dependent on viral replication. Nonviral methods for tumor-targeted delivery of immune-checkpoint inhibitors have also been reported. For example, microneedle patch-assisted delivery of anti–PD-1 induces robust immune responses in a B16F10 mouse melanoma model, but assessments of systemic immunity or toxicity were not performed (13). Direct intratumoral delivery also presents significant challenges in clinical implementation, and its therapeutic benefit is largely dependent on abscopal effects to treat metastatic lesions. To our knowledge, our report is the first to characterize the effects of conditional PD-1/PD-L1 checkpoint inhibitors on tumors and on systemic immunity and T-cell function.

We report the nonclinical activity of PD-1/L1 Pb-Tx, which have been designed to localize checkpoint inhibition to the tumor microenvironment and avoid the toxicities of systemic checkpoint blockade. This series of studies shows that Pb-Tx targeting either PD-1 or PD-L1 have antitumor activity similar to that of the corresponding unmasked mAb in a syngeneic mouse tumor model, both as monotherapy and in combination with anti–CTLA-4, and induce durable antitumor immunity. This is despite the fact that their systemic effect is markedly attenuated, as shown by reduced binding to circulating T cells and reduced ability to induce early-onset autoimmune diabetes in the NOD mouse. Furthermore, we have demonstrated that the protease-rich tumor microenvironment can activate sufficient levels of a Pb-Tx to elicit antitumor activity while low levels of systemic activity are maintained. To our knowledge, these data are the first to directly demonstrate that localizing PD-1/PD-L1 pathway inhibition to the tumor microenvironment can both induce effective antitumor immunity and minimize systemic PD-1/PD-L1 pathway blockade and associated toxicity.

Although we have described the activity of PD-1/PD-L1 Pb-Tx in a single checkpoint inhibitor–responsive syngeneic model in this report, we have previously reported the activity of a CD166-specific Pb-Tx in a set of 198 transplantable patient-derived xenograft (PDX) tumor models (40). The PDX study provides a robust data set demonstrating the activity of Pb-Tx in multiple preclinical models derived from a broad set of indications. Lastly, the PD-L1–targeted Pb-Tx CX-072, described here, has clinical activity in multiple cancer types including cutaneous squamous cell carcinoma (ORR = 36%), cancers with high tumor mutational burden (ORR = 29%), anal squamous cell carcinoma (SCC; ORR = 15%) and triple-negative breast cancer (ORR = 18%; refs. 41, 42). Taken together, the data indicate that Pb-Tx can become activated in tumors as designed and elicit the expected mechanism of action.

The primary limitation of the Pb-Tx experimental approach to test if tumor-localized inhibition of the PD-1/PD-L1 pathway is sufficient for effective antitumor immunity is that some minimal peripheral Pb-Tx activation can be detected. To evaluate the significance of this, we measured the level of circulating T cells bound with either the PD-L1 antibody or PD-L1 Pb-Tx in the blood of MC38 tumor–bearing mice. Peripheral blood $CD4^+$ T cells were analyzed by flow cytometry using a secondary antibody to detect bound PD-L1 antibody or Pb-Tx. We observed dose-dependent receptor occupancy of the surface PD-L1 with the PD-L1 antibody, but this occurred only at significantly higher exposures of the PD-L1 Pb-Tx. This identified a concentration of PD-L1 antibody where circulating T cells have nearly 100% PD-L1 receptor occupancy; at that same concentration of PD-L1 Pb-Tx, we observed minimal receptor occupancy of the recirculating lymphocytes. This suggests that at doses wherein we observed antitumor activity of the PD-L1 Pb-Tx, only a small population of T cells with PD-L1 bound Pb-Tx is observed in peripheral blood. Consistent with the receptor occupancy results, our data show that Pb-Tx significantly reduced peripheral PD-1/L1 blockade to levels insufficient to promote acceleration of autoimmune diabetes in a highly sensitive model of autoimmunity, despite equivalent antitumor immunity to an unmasked antibody. Collectively, these data suggest that localized inhibition of the PD-1/PD-L1 pathway in tumors is achievable with Pb-Tx, is sufficient for effective antitumor immunity, and reduces induction of systemic autoimmunity.

The limited response rates observed for cancer patients treated with single-agent PD-1/PD-L1 or CTLA-4 blocking antibodies remain a challenge for clinicians. To extend the benefit of immunotherapy to more patients, the field is moving toward combination therapy, with >3,000 clinical trials in progress involving checkpoint inhibitors (43). Although many of these combinations elicit an improved response compared with monotherapy, the adverse event profiles are often worsened. The most notable example is the combination of nivolumab (anti–PD-1) and ipilimumab (anti–CTLA-4), which produced objective response rates of 58% in a cohort of 314 previously untreated patients with melanoma and 42% in patients with advanced renal cell carcinoma (44–46). However, this improved efficacy came at the cost of serious immune-related adverse events, with both trials reporting grade 3 or 4 treatment-related adverse events in 45% to 55% of patients. Furthermore, a trial evaluating the combination of pembrolizumab and pegylated interferon (IFN) reported grade 3 or 4 treatment-related adverse events in 49% of patients (47, 48). The decreased tolerability of

Published OnlineFirst October 11, 2021; DOI: 10.1158/2326-6066.CIR-21-0031

checkpoint inhibitors when combined with additional immunomodulatory drugs can often result in patients discontinuing treatment, which may lower efficacy. These clinical results underscore the challenges in combining PD-1/PD-L1 with other immunostimulatory agents and emphasize the need for immunotherapies that are more effective and less toxic.

Our strategy of using Pb-Tx to effectively localize therapy to the tumor microenvironment and lessen systemic toxicity is currently being tested in several clinical trials. As seen in our nonclinical models, tumor protease content capable of activating therapeutic concentrations of PD-L1 Pb-Tx is observed in human tumor biopsies from our CX-072 clinical trials (49). Those data describe a dose-dependent increase in activated CX-072 Pb-Tx in human tumor biopsies, and concomitant evidence of checkpoint inhibition, as shown by an increase in tumor-infiltrating $CD8^+$ T cells. Preliminary phase I/II clinical evaluation of CX-072 (NCT03993379) has demonstrated antitumor activity consistent with the activity of other PD-1/PD-L1 pathway inhibitors but with a favorable safety profile, both as monotherapy and in combination (15, 41, 42). Clinical trials investigating a CTLA-4–targeting Pb-Tx (NCT03993379 and NCT03369223) in addition to trials investigating Pb-Tx directed against CD166 (NCT03149549) and transferrin receptor/CD71 (NCT03543813) are currently ongoing in monotherapy and combination settings.

Authors' Disclosures

K.A. Tipton reports other support from CytomX Therapeutics, Inc. during the conduct of the study, as well as a patents pending to CytomX Therapeutics, Inc. B. Howng is an employee and stockholder of CytomX Therapeutics, Inc. O. Vasiljeva is an employee of CytomX Therapeutics, Inc. D. Daniel reports personal fees from CytomX Therapeutics, Inc. outside the submitted work. W.M. Kavanaugh reports multiple patents pending and issued to CytomX Therapeutics, Inc., and has been an employee and is a stockholder of CytomX Therapeutics, Inc., which funded this work and receives advisory fees from multiple biotech companies. No disclosures were reported by the other authors.

Authors' Contributions

H.H. Assi: Conceptualization, validation, writing–original draft, project administration, writing–review and editing. **C. Wong:** Conceptualization, validation, project administration. **K.A. Tipton:** Conceptualization, validation, project administration. **L. Mei:** Conceptualization, resources. **K. Wong:** Investigation. **J. Razo:** Investigation. **C. Chan:** Conceptualization, resources, validation. **B. Howng:** Investigation. **J. Sagert:** Conceptualization, resources, validation. **M. Krimm:** Investigation. **L. Diep:** Conceptualization, resources, validation. **A. Jang:** Conceptualization, resources, validation. **M.T. Nguyen:** Investigation. **N. Lapuyade:** Conceptualization, resources, validation. **V. Singson:** Investigation. **R. Villanueva:** Investigation. **M. Paidhungat:** Conceptualization. **S. Liu:** Conceptualization. **V. Rangan:** Conceptualization, resources. **O. Vasiljeva:** Conceptualization, writing–original draft, writing–review and editing. **J.W. West:** Conceptualization. **J.H. Richardson:** Conceptualization, writing–original draft, writing–review and editing. **B. Irving:** Conceptualization. **D. Daniel:** Conceptualization, writing–original draft, writing–review and editing. **M. Belvin:** Conceptualization, writing–original draft, writing–review and editing. **W.M. Kavanaugh:** Conceptualization, writing–original draft, writing–review and editing.

Acknowledgments

These studies were sponsored by CytomX Therapeutics, Inc. Editorial assistance for preparing the manuscript was provided by Echelon Brand Communications, an OPEN Health company, Parsippany, NJ, and Twist Medical LLC, Burlingame, CA, and was funded by CytomX Therapeutics, Inc. PROBODY is a U.S. registered trademark of CytomX Therapeutics, Inc. All other brands and trademarks referenced herein are the property of their respective owners.

The costs of publication of this article were defrayed in part by the payment of page charges. This article must therefore be hereby marked *advertisement* in accordance with 18 U.S.C. Section 1734 solely to indicate this fact.

Received January 13, 2021; revised May 28, 2021; accepted October 8, 2021; published first October 11, 2021.

References

1. Alsaab HO, Sau S, Alzhrani R, Tatiparti K, Bhise K, Kashaw SK, et al. PD-1 and PD-L1 checkpoint signaling inhibition for cancer immunotherapy: mechanism, combinations, and clinical outcome. Front Pharmacol 2017;8:561.
2. Topalian SL, Sznol M, McDermott DF, Kluger HM, Carvajal RD, Sharfman WH, et al. Survival, durable tumor remission, and long-term safety in patients with advanced melanoma receiving nivolumab. J Clin Oncol 2014;32:1020–30.
3. Bajwa R, Cheema A, Khan T, Amirpour A, Paul A, Chaughtai S, et al. Adverse effects of immune checkpoint inhibitors (programmed death-1 inhibitors and cytotoxic T-lymphocyte-associated protein-4 inhibitors): results of a retrospective study. J Clin Med Res 2019;11:225–36.
4. Wolchok JD, Kluger H, Callahan MK, Postow MA, Rizvi NA, Lesokhin AM, et al. Nivolumab plus ipilimumab in advanced melanoma. N Engl J Med 2013;369:122–33.
5. Anderson R, Theron AJ, Rapoport BL. Immunopathogenesis of immune checkpoint inhibitor-related adverse events: roles of the intestinal microbiome and Th17 cells. Front Immunol 2019;10:2254.
6. Cadranel J, Canellas A, Matton L, Darrason M, Parrot A, Naccache JM, et al. Pulmonary complications of immune checkpoint inhibitors in patients with nonsmall cell lung cancer. Eur Respir Rev 2019;28:190058.
7. Geukes Foppen MH, Rozeman EA, van Wilpe S, Postma C, Snaebjornsson P, van Thienen JV, et al. Immune checkpoint inhibition-related colitis: symptoms, endoscopic features, histology and response to management. ESMO Open 2018;3:e000278.
8. Iwai Y, Terawaki S, Ikegawa M, Okazaki T, Honjo T. PD-1 inhibits antiviral immunity at the effector phase in the liver. J Exp Med 2003;198:39–50.
9. Wiendl H, Mitsdoerffer M, Schneider D, Chen L, Lochmuller H, Melms A, et al. Human muscle cells express a B7-related molecule, B7-H1, with strong negative immune regulatory potential: a novel mechanism of counterbalancing the immune attack in idiopathic inflammatory myopathies. FASEB J 2003;17:1892–4.
10. Puzanov I, Diab A, Abdallah K, Bingham CO 3rd,Brogdon C, Dadu R, et al. Managing toxicities associated with immune checkpoint inhibitors: consensus recommendations from the Society for Immunotherapy of Cancer (SITC) Toxicity Management Working Group. J Immunother Cancer 2017;5:95.
11. Zhang B, Wu Q, Zhou YL, Guo X, Ge J, Fu J. Immune-related adverse events from combination immunotherapy in cancer patients: a comprehensive meta-analysis of randomized controlled trials. Int Immunopharmacol 2018;63:292–8.
12. Bartee MY, Dunlap KM, Bartee E. Tumor-localized secretion of soluble PD1 enhances oncolytic virotherapy. Cancer Res 2017;77:2952–63.
13. Wang C, Ye Y, Hochu GM, Sadeghifar H, Gu Z. Enhanced cancer immunotherapy by microneedle patch-assisted delivery of anti-PD1 antibody. Nano Lett 2016;16:2334–40.
14. Spitzer MH, Carmi Y, Reticker-Flynn NE, Kwek SS, Madhireddy D, Martins MM, et al. Systemic immunity is required for effective cancer immunotherapy. Cell 2017;168:487–502.
15. Autio KA, Boni V, Humphrey RW, Naing A. Probody therapeutics: an emerging class of therapies designed to enhance on-target effects with reduced off-tumor toxicity for use in immuno-oncology. Clin Cancer Res 2020;26:984–9.
16. Kavanaugh WM. Antibody prodrugs for cancer. Expert Opin Biol Ther 2020;20:163–71.
17. Desnoyers LR, Vasiljeva O, Richardson JH, Yang A, Menendez EE, Liang TW, et al. Tumor-specific activation of an EGFR-targeting probody enhances therapeutic index. Sci Transl Med 2013;5:207ra144.
18. Turk B. Targeting proteases: successes, failures and future prospects. Nat Rev Drug Discov 2006;5:785–99.
19. LeBeau AM, Lee M, Murphy ST, Hann BC, Warren RS, Delos Santos R, et al. Imaging a functional tumorigenic biomarker in the transformed epithelium. Proc Natl Acad Sci 2013;110:93–8.

Published OnlineFirst October 11, 2021; DOI: 10.1158/2326-6066.CIR-21-0031

20. Ji M, Li S, Xie Y, Zhao Z, Chang W, Li Y, et al. Expression and prognostic value of matriptase in ovarian serous adenocarcinoma. Oncol Lett 2017;13:1741–44.
21. Gobin E, Bagwell K, Wagner J, Mysona D, Sandirasegarane S, Smith N, et al. A pan-cancer perspective of matrix metalloproteases (MMP) gene expression profile and their diagnostic/prognostic potential. BMC Cancer 2019;19:581.
22. Vasiljeva O, Hostetter DR, Moore SJ, Winter MB. The multifaceted roles of tumor-associated proteases and harnessing their activity for prodrug activation. Biol Chem 2019;400:965–77.
23. Erster O, Thomas JM, Hamzah J, Jabaiah AM, Getz JA, Schoep TD, et al. Site-specific targeting of antibody activity in vivo mediated by disease-associated proteases. J Control Release 2012;161:804–12.
24. Wong C, Mei L, Wong KR, Menendez EEM, Vasiljeva O, Richardson JH, et al. A PD-L1-targeted Probody provides antitumor efficacy while minimizing induction of systemic autoimmunity [abstract]. In: Proceedings of the CRI-CIMT-EATI-AACR Inaugural International Cancer Immunotherapy Conference: Translating Science into Survival; 2015 Sep 16–19; New York, NY. Philadelphia (PA): AACR; Cancer Immunol Res 2016;4(1 Suppl):Abstract nr A081.
25. Butte MJ, Keir ME, Phamduy TB, Sharpe AH, Freeman GJ. Programmed death-1 ligand 1 interacts specifically with the B7–1 costimulatory molecule to inhibit T cell responses. Immunity 2007;27:111–22.
26. Freeman GJ, Long AJ, Iwai Y, Bourque K, Chernova T, Nishimura H, et al. Engagement of the PD-1 immunoinhibitory receptor by a novel B7 family member leads to negative regulation of lymphocyte activation. J Exp Med 2000; 192:1027–34.
27. Wang C, Thudium KB, Han M, Wang XT, Huang H, Feingersh D, et al. In vitro characterization of the anti-PD-1 antibody nivolumab, BMS-936558, and in vivo toxicology in non-human primates. Cancer Immunol Res 2014;2:846–56.
28. Rice JJ, Schohn A, Bessette PH, Boulware KT, Daugherty PS. Bacterial display using circularly permuted outer membrane protein OmpX yields high affinity peptide ligands. Protein Sci 2006;15:825–36.
29. Agata Y, Kawasaki A, Nishimura H, Ishida Y, Tsubata T, Yagita H, et al. Expression of the PD-1 antigen on the surface of stimulated mouse T and B lymphocytes. Int Immunol 1996;8:765–72.
30. Tipton KA, Chan C, Wong KR, Singson V, Richardson JH, Kavanaugh WM, et al. PD-1-targeted Probody therapeutics provide anti-tumor efficacy and a 10-fold dose protection against systemic autoimmunity in preclinical studies [abstract]. In: Proceedings of the 107th Annual Meeting of the American Association for Cancer Research; 2016 Apr 16–20; New Orleans, LA. Philadelphia (PA): AACR; Cancer Res 2016;76(14 Suppl):Abstract nr 3211.
31. Tipton KA, Wong KR, Singson V, Wong C, Chan C, Huang Y, et al. Probody therapeutics targeting the PD-1/L1 axis provide preclinical anti-tumor efficacy while minimizing induction of autoimmunity as single agents and in combination with CTLA-4 blockade. J Immunother Cancer 2016;4(Suppl 1):120–1. Abstract nr P213.
32. Selby MJ, Engelhardt JJ, Johnston RJ, Lu LS, Han M, Thudium K, et al. Preclinical development of ipilimumab and nivolumab combination immunotherapy: mouse tumor models, in vitro functional studies, and cynomolgus macaque toxicology. PLoS One 2016;11:e0161779.
33. Giesen D, Broer LN, Lub-de Hooge MN, Popova I, Howng B, Nguyen M, et al. Probody therapeutic design of 89Zr-CX-072 promotes accumulation in PD-L1 expressing tumors compared to normal murine lymphoid tissue. Clin Cancer Res 2020;26:3999–4009.
34. Paterson AM, Brown KE, Keir ME, Vanguri VK, Riella LV, Chandraker A, et al. The programmed death-1 ligand 1:B7-1 pathway restrains diabetogenic effector T cells in vivo. J Immunol 2011;187:1097–105.
35. Ansari MJ, Salama AD, Chitnis T, Smith RN, Yagita H, Akiba H, et al. The programmed death-1 (PD-1) pathway regulates autoimmune diabetes in non-obese diabetic (NOD) mice. J Exp Med 2003;198:63–9.
36. Luhder F, Hoglund P, Allison JP, Benoist C, Mathis D. Cytotoxic T lymphocyte-associated antigen 4 (CTLA-4) regulates the unfolding of autoimmune diabetes. J Exp Med 1998;187:427–32.
37. Engeland CE, Grossardt C, Veinalde R, Bossow S, Lutz D, Kaufmann JK, et al. CTLA-4 and PD-L1 checkpoint blockade enhances oncolytic measles virus therapy. Mol Ther 2014;22:1949–59.
38. Kleinpeter P, Fend L, Thioudellet C, Geist M, Sfrontato N, Koerper V, et al. Vectorization in an oncolytic vaccinia virus of an antibody, a Fab and a scFv against programmed cell death -1 (PD-1) allows their intratumoral delivery and an improved tumor-growth inhibition. Oncoimmunology 2016;5: e1220467.
39. Reul J, Frisch J, Engeland CE, Thalheimer FB, Hartmann J, Ungerechts G, et al. Tumor-specific delivery of immune checkpoint inhibitors by engineered AAV vectors. Front Oncol 2019;9:52.
40. Liu BY, Shen J, Will M, Yalamanchili S, Ford-Gordon J, Stroh K, et al. CD166-DM4 Probody™ drug conjugate (CX-2009) treatment of 198 patient-derived xenograft models (PDX) in a mouse clinical trial format [abstract]. In: Proceedings of the American Association for Cancer Research Annual Meeting 2019; 2019 Mar 29–Apr 3; Atlanta, GA. Philadelphia (PA): AACR; Cancer Res 2019;79 (13 Suppl):Abstract nr 212.
41. Sanborn RE, Hamid O, de Vries EG, Ott PA, Garcia-Corbacho J, Boni V, et al. CX-072 (pacmilimab), a Probody PD-L1 inhibitor, in combination with ipilimumab in patients with advanced solid tumors (PROCLAIM-CX-072): a first-in-human, dose-finding study. J Immunother Cancer 2021;9: e002446.
42. Naing A, Thistlethwaite F, De Vries EGE, Eskens FALM, Uboha N, Ott PA, et al. CX-072 (pacmilimab), a Probody® PD-L1 inhibitor, in advanced or recurrent solid tumors (PROCLAIM-CX-072): an open-label dose-finding and first-in-human study. J Immunother Cancer 2021;9:e002447.
43. Schmidt EV. Developing combination strategies using PD-1 checkpoint inhibitors to treat cancer. Semin Immunopathol 2019;41:21–30.
44. Larkin J, Chiarion-Sileni V, Gonzalez R, Grob JJ, Cowey CL, Lao CD, et al. Combined nivolumab and ipilimumab or monotherapy in untreated melanoma. N Engl J Med 2015;373:23–34.
45. Larkin J, Chiarion-Sileni V, Gonzalez R, Grob JJ, Rutkowski P, Lao CD, et al. Five-year survival with combined nivolumab and ipilimumab in advanced melanoma. N Engl J Med 2019;381:1535–46.
46. Motzer RJ, Tannir NM, McDermott DF, Aren Frontera O, Melichar B, Choueiri TK, et al. Nivolumab plus ipilimumab versus sunitinib in advanced renal-cell carcinoma. N Engl J Med 2018;378:1277–90.
47. Atkins MB, Hodi FS, Thompson JA, McDermott DF, Hwu WJ, Lawrence DP, et al. Pembrolizumab plus pegylated interferon alfa-2b or ipilimumab for advanced melanoma or renal cell carcinoma: dose-finding results from the phase Ib KEYNOTE-029 study. Clin Cancer Res 2018;24:1805–15.
48. Davar D, Wang H, Chauvin JM, Pagliano O, Fourcade JJ, Ka M, et al. Phase Ib/II study of pembrolizumab and pegylated-interferon alfa-2b in advanced melanoma. J Clin Oncol 2018;36:3450–8.
49. Lyman S, Naing A, Zein IA, Ru Y, Howng B, Winter MB, et al. Evidence of intratumoral localization, activation, and immunomodulatory effect of CX-072, a probody therapeutic targeting PD-L1, in a phase I/II trial. J Clin Oncol 38: 2020 (suppl; abstr 3108).

AACR American Association for Cancer Research

Cancer Immunology Research

Conditional PD-1/PD-L1 Probody Therapeutics Induce Comparable Antitumor Immunity but Reduced Systemic Toxicity Compared with Traditional Anti–PD-1/PD-L1 Agents

Hikmat H. Assi, Chihunt Wong, Kimberly A. Tipton, et al.

Cancer Immunol Res Published OnlineFirst October 11, 2021.